ARTICLES
https://doi.org/10.1038/s41565-020-00825-9
nature nanotechnology

Ion-exchange enabled synthetic swarm

Changjin Wu[1,6], Jia Dai[1,6], Xiaofeng Li[1], Liang Gao[2], Jizhuang Wang[1], Jun Liu[1], Jing Zheng[1], Xiaojun Zhan[1], Jiawei Chen[1], Xiang Cheng[1], Mingcheng Yang[3,4] ✉ and Jinyao Tang[1,5] ✉

Active matters are out-of-equilibrium systems that convert energy from the environment to mechanical motion. Non-reciprocal interaction between active matters may lead to collective intelligence beyond the capability of individuals. In nature, such emergent behaviours are ubiquitously observed in animal colonies, giving these species remarkable adaptive capability. In artificial systems, however, the emergence of non-trivial collective intelligent dynamics remains undiscovered. Here we show that a simple ion-exchange reaction can couple self-propelled ZnO nanorods and sulfonated polystyrene microbeads together. Chemical communication is established that enhances the reactivity and motion of both nanorods and the microbeads, resulting in the formation of an active swarm of nanorod–microbead complexes. We demonstrate that the swarm is capable of macroscopic phase segregation and intelligent consensus decision-making.

Complex systems are composed of an ensemble of elementary components without central control, where non-trivial collective behaviours, intricate information processing and adaptation emerge. Schools of fish, flocks of birds and bacterial colonies are examples of complex systems in nature[1–3]. Recently, synthetic active matter has aroused interest due to its potential in biomedical applications[4–6], as well as serving as the perfect model system for non-equilibrium physics[7–9]. Notably, highly functional active nanoparticles have been proposed as minuscule robots for complex tasks. However, due to the limited size, it is challenging to incorporate sophisticated logic circuits into individual active particles[10], limiting their functionality. Therefore, the collective intelligence emerging from the interaction network of millions of individual simple particles should be explored to enable advanced functions. The collective intelligence of assembled individuals is ubiquitous in nature; for instance, a solitary army ant shows limited individual intelligence, as it merely follows its neighbours. However, as millions of individual ants group together, the ant colony acts as a 'superorganism' with superb collective intelligence, where complicated tasks such as effective territory exploration or building bridges can be accomplished[11].

Inspired by the microbial symbiosis system[12–14], here, we demonstrate a minimal complex system composed of two chemically coupled species, where the 'waste' product of one is the 'nutrient' for another. This chemical coupling establishes a communication-dependent activity for both particle species, which results in the emergence of sophisticated dynamic self-organization and consensus decision-making behaviour. A coarse-grained model shows that both interparticle osmotic interactions and the separation-dependent activity are essential to the observed collective intelligence.

ZnO nanorods and sulfonated polystyrene as active particles

As conceptually illustrated in Fig. 1a, two chemically powered particles A and B release their own chemical 'waste' α and β, respectively, during their propulsion. On mixing, A and B interact with each other by exchanging 'waste' and 'nutrient'. The released 'waste' α from particle A is collected by particle B as its 'nutrient' and promotes its activity, while the same scenario also applies to the 'waste' β to particle A. To establish such exchange communication, we used what is arguably the simplest chemical reaction, the ion-exchange reaction. The self-propelled ZnO nanorod and chemically active sulfonated polystyrene (PS) microbeads are coupled together by exchanging ions. The ZnO and sulfonated PS form active complexes, where both repulsive and attractive interactions are regulated by the local ion concentration that is contributed by all nearby particles.

Figure 1b shows the ZnO nanorod crystal structure along the [0001] direction with Zn-terminated (0001) Zn polar surface. The Zn-terminated polar facet has higher surface energy and preferentially dissolves and releases Zn^{2+} and OH^- into the solution[15,16], which propels the nanorod by self-diffusiophoresis (schematic diagram in Fig. 1c). As shown in Fig. 1c, the as-prepared ZnO nanorods (see Supplementary Information for the synthesis process) can migrate in deionized water at speed of roughly $2\,\mu m\,s^{-1}$ (Supplementary Video 1a), which lasts for more than 30 mins. The facet selective etching of ZnO nanorod is confirmed by the appearance of a void on the ZnO nanorod end, as shown in the inset of Fig. 1c. This continuous end facet dissolution leads to diffusiophoretic propulsion along the nanorod axis, while the surface flaws on the ZnO nanorod sidewalls serve as an additional dissolution site and steer the migration in a circle for some nanorods. In contrast, those nanorods with smooth sidewalls move following a straight trajectory (Supplementary Fig. 2). As the dissolution rate of ZnO is highly pH dependent[17], the ZnO nanorod is inherently a pH-responsive microswimmer[18,19]. The acidic environment will strongly increase the activity of ZnO and enhance its motion.

The cationic ion exchangers absorb cations in solution and release H^+, which is widely used in water treatment. It has been reported that, due to the different mobility of the adsorbed and released ions, the ion exchanger microspheres could generate an ionic gradient and attract each other by the self-generated electroosmotic flow on the substrate[20,21].

[1]Department of Chemistry, The University of Hong Kong, Hong Kong, China. [2]School of Chemical Engineering and Light Industry, Guangdong University of Technology, Guangzhou, China. [3]Beijing National Laboratory for Condensed Matter Physics and Laboratory of Soft Matter Physics, Institute of Physics, Chinese Academy of Sciences, Beijigng, China. [4]School of Physical Sciences, University of Chinese Academy of Sciences, Beijing, China. [5]State Key Laboratory of Synthetic Chemistry, The University of Hong Kong, Hong Kong, China. [6]These authors contributed equally: Changjin Wu, Jia Dai.
✉e-mail: mcyang@iphy.ac.cn; jinyao@hku.hk

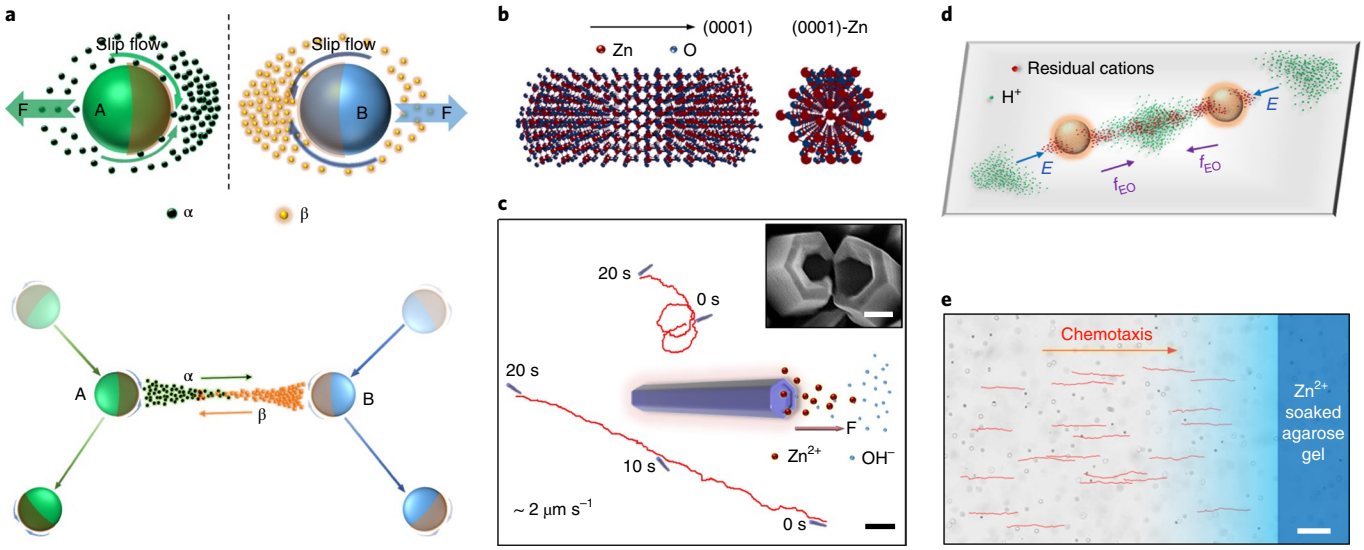

Fig. 1 | The exchange communication between different microswimmer species and the model system used in this study. a, Schematic illustration of two independent active particles A and B, where the black dot α and yellow dot β denote the released chemical 'waste' from A and B, respectively. The asymmetric chemical gradients induce slip flow at the surface of A and B, which propel the particles. In the case of exchange interaction, particles A and B are coupled together by exchanging chemical signal α and β. **b**, Illustration of the ZnO nanorod crystal structure, which dissolves preferentially at (0001) plane. **c**, Illustration of the asynchronized diffusion of Zn^{2+} and OH^- propel the ZnO nanorod and the observed migration trajectories of ZnO nanorod in deionized water within 20 s. Inset shows the ZnO nanorod etching cavity at the end facet. **d**, Schematic diagram of the electroosmotic interaction between sulfonated PS. The overlapped gradients of residual cations and released H^+ form an asymmetric electric field E and subsequent asymmetric electroosmotic flow f_{EO}, which promote the assembly of sulfonated PS. **e**, Sulfonated PS migrate towards the Zn^{2+}-soaked agarose gel via the positive chemotaxis (the red lines are the trajectories of sulfonated PS). Scale bars 4 μm (**c**), 400 nm (inset of **c**) and 60 μm (**e**).

In our experiment, the monodispersed sulfonated PS microbeads (see Supplementary Information for the synthesis process) were used as ion exchangers to interact with the ZnO swimmer. In general, active particles refer to particles that convert energy from the surroundings into mechanical work at the individual level. In this sense, the symmetric sulfonated PS microbead is mechanically passive as it cannot self-propel without symmetry breaking. However, a sulfonated PS microbead is chemically active as an ion exchanger and can generate osmotic flow around itself along the substrate. As a result, this osmotic flow mechanically interacts with other sulfonated PS microbeads in a crowded environment[20,22], which also creates mechanical motion at the ensembled level. As illustrated in Fig. 1d and Supplementary Video 1b, the sulfonated PS microbeads (diameter roughly 1.5 μm) in water generate symmetric ionic gradients, which overlap with the ionic gradients from neighbouring particles. The consequent osmosis interaction assembles the sulfonated PS microbeads into dimers, trimers, chains and eventually into clusters (Supplementary Fig. 4a) via the reaction:

$$PS-SO_3H + M^+ \rightleftharpoons PS-SO_3M + H^+ \quad (1)$$

A similar phenomenon has been previously observed with commercial cationic ion-exchange resin particles with a larger diameter (roughly 15 μm)[20], while our sulfonated PS microbeads have a smaller diameter and larger surface area to volume ratio, which enables greater ion-exchange capacity (Supplementary Table 1) and higher mobility by enhancing the exchange rate. Therefore, a longer reaction lifetime was observed when interacting with ZnO, which is essential to the collective emergence.

As the sulfonated PS microbeads deplete the cations in solution, the migration speed correspondingly decreases from 2.5 to roughly 1 μm s^{-1} in 100 s (Supplementary Fig. 4b). Since the chemical reaction in equation (1) is thermodynamically spontaneous, the positive chemotaxis is observed for the sulfonated PS microbead by placing a Zn^{2+} soaked agarose gel inside the solution to generate the Zn^{2+} concentration gradient (Fig. 1e, Supplementary Video 1c and Supplementary Information for the detailed experimental process), which could be attributed to the Zn^{2+} gradient-induced diffusiophoresis and asymmetric ion exchange.

Ion-exchange interaction between ZnO nanorod and sulfonated PS microbead

On the basis of the aforementioned active particles, the reactions for ZnO nanorod and sulfonated PS microbead propulsion can be easily coupled as:

$$\text{ZnO nanorod: } ZnO_{(s)} + H_2O_{(l)} \rightleftharpoons Zn^{2+}_{(aq)} + 2OH^-_{(aq)} \quad (2)$$

Sulfonated PS:

$$2PS-SO_3H_{(s)} + Zn^{2+}_{(aq)} \rightleftharpoons 2(PS-SO_3)_2Zn_{(s)} + 2H^+_{(aq)} \quad (3)$$

$$H_2O\ \text{self}-\text{ionization: } H^+_{(aq)} + OH^-_{(aq)} = H_2O_{(l)} \quad (4)$$

Overall reaction:

$$ZnO_{(s)} + 2PS-SO_3H_{(s)} = (PS-SO_3)_2Zn_{(s)} + H_2O_{(l)} \quad (5)$$

As illustrated in Fig. 2a, via the ion-exchange reaction, two active particle species are coupled together, which enables the synergistic interaction. It is observed that the migration speeds of both ZnO nanorods and sulfonated PS microbeads are strongly regulated by the nearby counter particles, where great enhancement is achieved. In this system, the ZnO nanorod serves as a local Zn^{2+} source, which chemotactically attracts surrounding sulfonated PS microbeads. As the sulfonated PS microbead approaching ZnO nanorod, the speed

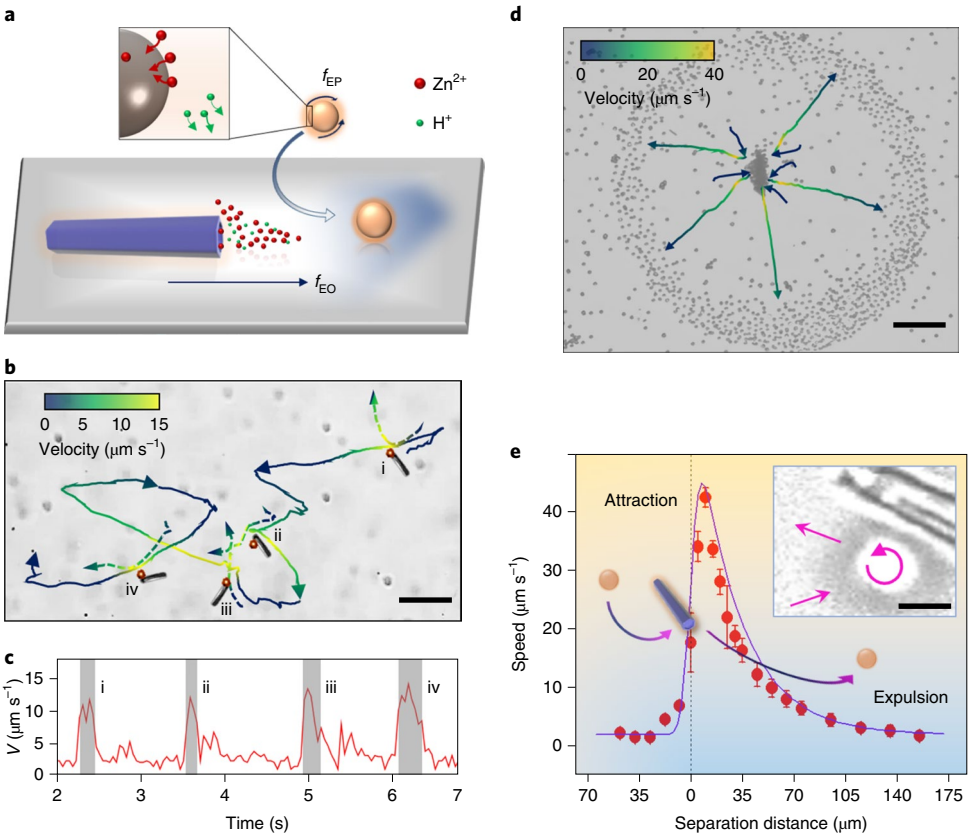

Fig. 2 | The ion-exchange interaction between ZnO nanorod and sulfonated PS. a, Schematic diagram of the ion exchange between a ZnO nanorod and sulfonated PS. The sulfonated PS absorbs Zn^{2+} and releases H^+, while the ZnO nanorod consumes H^+ and generates Zn^{2+}. The sulfonated PS are propelled towards ZnO nanorods by electrophoretic flow f_{EP} and then are pushed away by the near-substrate electroosmotic flow f_{EO}. **b**, The trajectory of a single ZnO nanorod showing the enhanced propulsion by assembling with a sulfonated PS. Four assembly events (i, ii, iii, iv) are plotted in the trajectory, while the colour bar represents the speed of the ZnO nanorod. **c**, The migration speed of the corresponding ZnO nanorod is shown in **b**, where the shaded speed spikes correspond to the transient ZnO assembly with the sulfonated PS. **d**, ZnO–sulfonated PS complex formation with an immobilized ZnO nanorod, where the trajectories of the sulfonated PS are coloured corresponding to their instant speeds. **e**, Relationship of the speed of sulfonated PS with their separation distance from the ZnO nanorod. The error bars represent the standard deviation of the speed from multiple particles ($n = 50$). Inset shows the magnified confocal microscope image of the sulfonated PS particle first attracted then expelled by ZnO, while constantly spinning near the ZnO surface. Scale bars 20 μm (**b**), 30 μm (**d**), 1.5 μm (inset of **e**).

of sulfonated PS microbead increases due to the higher Zn^{2+} concentration; in turn, the H^+ released from sulfonated PS microbead accelerates the ZnO propulsion by lowering the local pH, which further boosts the Zn^{2+} concentration gradient. Consequently, this positive feedback enhances the propulsion of both ZnO nanorod and sulfonated PS microbead. On the assembly of the sulfonated PS microbead with the ZnO nanorod, a transient ZnO–sulfonated PS complex is formed, where the strong ion-exchange interaction dramatically enhances the migration speed of the complex (Fig. 2b and Supplementary Video 2a). As shown in Fig. 2a, the outward electroosmotic flow along the glass substrate from the ZnO nanorod disassembles the ZnO–sulfonated PS complex and leads to the pulsed speed of the ZnO nanorod, as shown in Fig. 2c.

This intriguing interaction can be more explicitly illustrated by the trajectories of sulfonated PS microbeads with the ZnO nanorod immobilized on the glass substrate. Figure 2d and Supplementary Video 3 show the formation of the active ZnO–sulfonated PS complex near the substrate. As shown in Supplementary Video 2b and the inset of Fig. 2e, after being attracted to the ZnO surface, the spinning sulfonated PS microbead assembles with the ZnO nanorod, possibly at the equilibrium position of the chemotaxis attraction and surface slipping flow around the ZnO nanorod, forming a quasi-stable complex. The beads are then expelled by the near-substrate outward electroosmotic flow. The continuous attraction and expulsion leads to a particle depletion zone around the ZnO nanorod (Fig. 2d), which can be regarded as the visualized Zn^{2+} diffusion region as the outward electroosmotic flow is created by the asynchronous Zn^{2+} and OH^- diffusion. Outside this region, most Zn^{2+} are consumed and converted to H^+, as confirmed with pH and Zn^{2+} concentration mapping from a confocal microscope (Supplementary Fig. 10a,c). As a result, the outward electroosmotic flow is suppressed and the attraction between sulfonated PS microbeads dominates, which leads to the aggregation of sulfonated PS microbeads around the ZnO nanorod (Fig. 2d and Supplementary Fig. 9).

Since the chemical gradients and fluid flow are in three dimensions, the particles also move in three dimensions. We tracked 400 sulfonated PS microbeads at four different heights ($Z = 0$, 6, 10, 14 μm) above the substrate. As shown in Fig. 3a, the migration speed of sulfonated PS microbead is sensitive to the ZnO–sulfonated PS distance at all heights, while the near-substrate ($Z < 6$ μm) outward migration is compensated by the inward migration over the substrate ($Z > 6$ μm). The three dimensional (3D) trajectories are also observed by 3D confocal microscope scanning (Fig. 3b

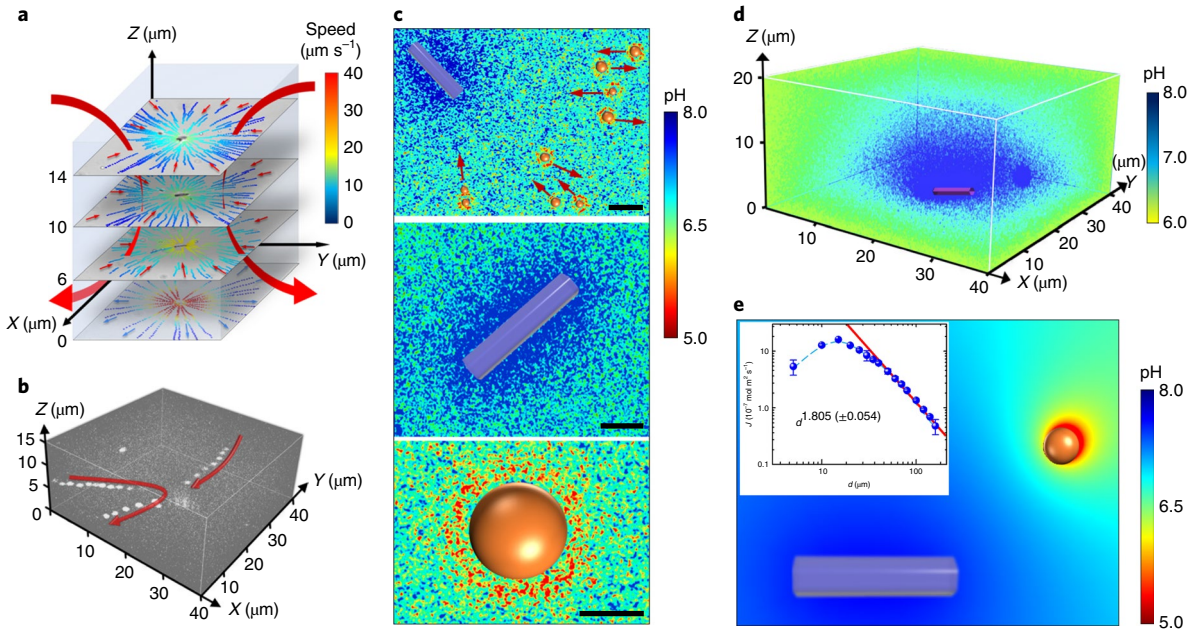

Fig. 3 | 3D velocity field and pH profile of the ZnO nanorod–sulfonated PS system. a, 3D velocity field with 400 trajectories of sulfonated PS at four heights ($Z = 0$, 6, 10, 14 μm) near a fixed ZnO nanorod ($Z = 0$ μm) shows the particles are attracted to the ZnO above the substrate before being expelled along the substrate. The colour map and the red arrows represent the speed and migration directions of sulfonated PS, respectively. **b**, 3D trajectories of sulfonated PS recorded by 3D scanning under the confocal microscope, where the red arrows represent the migration directions. **c**–**e**, Two-dimensional (**c**) and 3D (**d**) pH profiles measured by confocal microscope and compared with the numerical simulation (**e**) during the ion-exchange interaction between the ZnO nanorod and sulfonated PS. The red arrows in the upper part of **c** represent the instant migration direction of the given particles. The inset of **e** shows the power-law dependence between ion flux density and the interparticle distance, where the error bars are the standard deviation of multiple sulfonated PS ($n = 20$). Scale bars 5 μm (**c** upper image), 3 μm (**c** middle image), 1 μm (**c** lower image).

and Supplementary Video 4b). Although this attractive–repulsive interaction may also occur in the traditional active–passive particle system, the range and strength are dramatically enhanced with the ion-exchange interaction.

To further explain the aforementioned ion-exchange interaction, experimental and numerical simulated pH mapping were used to verify the reaction between the ZnO nanorod and sulfonated PS microbeads. We used a pH-sensitive fluorescent dye (5(6)-carboxyfluorescein) to probe in situ the local pH of the ZnO–sulfonated PS microbead system under a confocal microscope (Supplementary Information). As shown in the two-dimensional pH mapping in Fig. 3c, a higher pH (roughly 8.0) near the ZnO nanorod and lower pH close to the sulfonated PS microbeads (roughly 5.0) are observed. The 3D pH mapping clearly shows the 3D pH gradient near the ZnO nanorod (Fig. 3d and Supplementary Video 4a), while due to the fast motion of sulfonated PS microbeads, its nearby pH gradient cannot be captured in three dimensions. Nevertheless, this pH gradient universally exists around the ZnO and sulfonated PS as induced by the ion-exchange reaction. As explained in the interaction between an individual ZnO nanorod and sulfonated PS microbead, the release of Zn^{2+}/OH^- and consumption of H^+ by the ZnO nanorod together increase the local pH, while the generation of H^+ by the sulfonated PS microbead decreases the local pH.

This pH distribution and fluid field can be rationalized using the numerical simulation COMSOL (Supplementary Information), where the separation-dependent generation and consumption rate of Zn^{2+}, OH^- and H^+ for ZnO and the sulfonated PS microbead was set to match the experimentally observed migration speed. As shown in Fig. 3e and Supplementary Fig. 9, the pH and Zn^{2+} gradients generated in the simulation model are similar to the experimental observation. On the basis of the simulation, the power-law dependence of the interparticle distance to the particle reactivity can be evaluated. As shown in the inset of Fig. 3e, the activity, as qualified by the exchange ion flux density J, is dependent on the ZnO–sulfonated PS microbead distance (d) with the power rule roughly being 1.805 ± 0.054 (95% confidence level). This means that the ion-exchange activity can be roughly regarded as being inversely proportional to the square of the particle distance.

The above results demonstrate that the ion-exchange reaction is an effective way to generate communication-dependent coupling between a ZnO nanorod and sulfonated PS microbead, which distinguishes the ZnO–sulfonated PS system from other active particle systems in three ways. First, both ZnO nanorod and sulfonated PS microbead are chemically active, which differs from the interaction between an active particle and passive particle. This is shown in the control experiment where the Pt-coated 3-(trimethoxysilyl)propyl methacrylate (TPM) Janus active particle only weakly interacts with a passive PS particle at short range (Supplementary Fig. 7a and Supplementary Video 3). Second, due to the concentration-dependent ion-exchange reaction, the interaction of the ion-exchange particles is strongly regulated by their separation distances (Fig. 2e). Third, the ion-exchange reaction induces a strong electroosmotic interaction, where the inward osmotic flow (attractive osmosis) generated by sulfonated PS microbeads drives the assembly of neighbouring ZnO–sulfonated PS microbeads, while the outward osmotic flow (repulsive osmosis) produced by the ZnO nanorod repels the surrounding particles. These three distinctive features lead to complex dynamics of the ZnO–sulfonated PS mixture on a large scale and the emergence of non-trivial collective behaviours.

We believe the strong ion-exchange interaction is not unique to the ZnO–sulfonated PS system, but is ubiquitous as long as ions

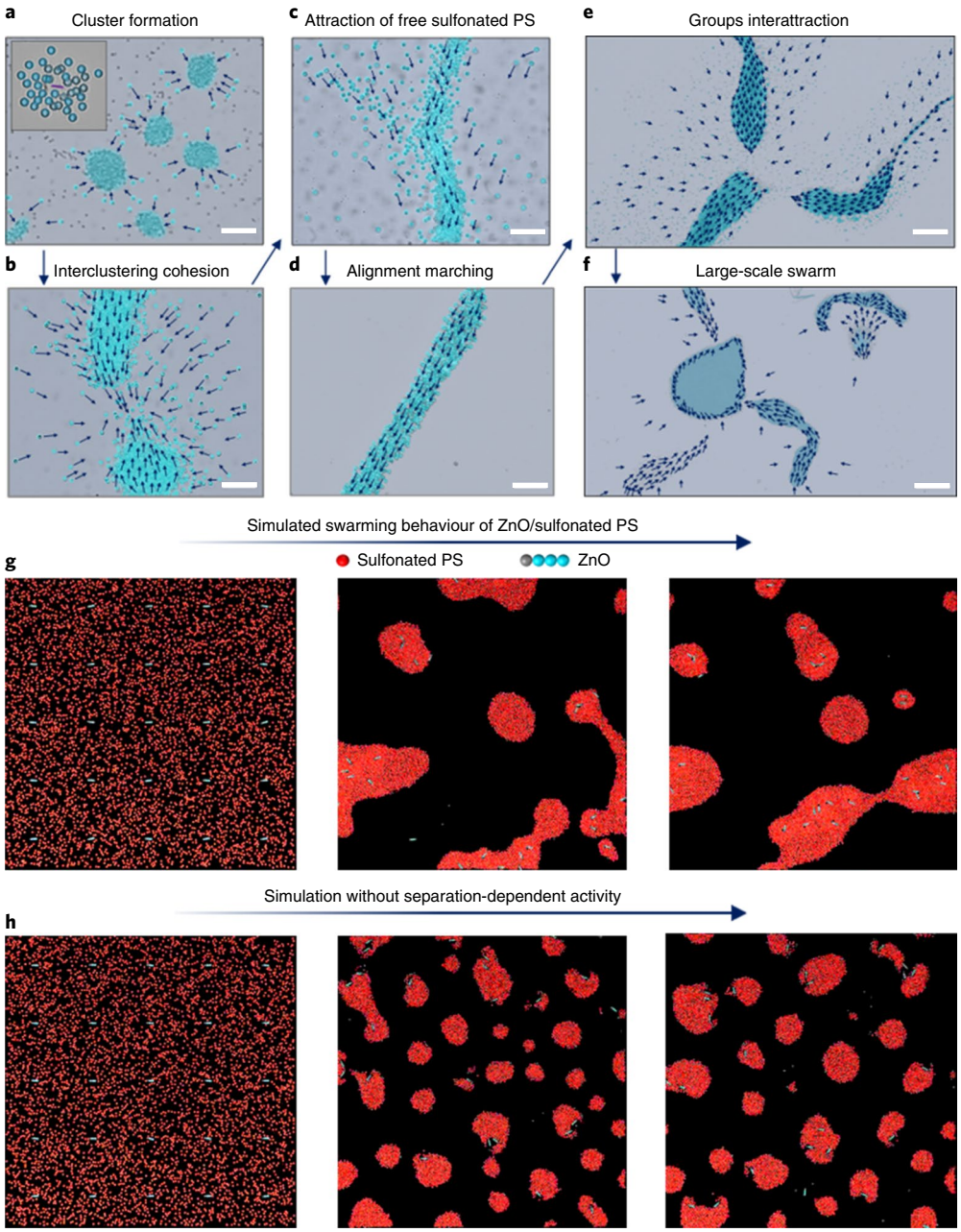

Fig. 4 | The emergence of swarming behaviour of ZnO–sulfonated PS mixture in experiment and simulation. a, Sulfonated PS accumulate around the ZnO nanorod and form clusters with the ZnO nanorod core (inset of **a**). **b**, Cohesion of adjacent ZnO nanorod–sulfonated PS clusters via attractive osmosis. **c**,**d**, Free sulfonated PS as well as ZnO–sulfonated PS clusters self-align (**c**) and alignment marching (**d**). **e**, ZnO–sulfonated PS clusters further aggregate. **f**, Large-scale swarming behaviour of the ZnO–sulfonated PS mixture. Particle densities, 0.3 μg ml^{-1} for the ZnO nanorod and 30 μg ml^{-1} for sulfonated PS particles. Scale bars, 50 μm (**a**), 20 μm (**b**,**c**,**d**), 200 μm (**e**) and 500 μm (**f**). **g**, Coarse-grained simulation result from the swarming behaviour of the ZnO–sulfonated PS mixture. The red balls represent the sulfonated PS and the four connected balls represent the ZnO nanorod. The grey ball of the ZnO nanorod represents the reactive facet, while the blue balls represent the inactive part. **h**, Coarse-grained simulation of the ZnO–sulfonated PS mixture without communication-dependent activity, which differs from **g** by fixing the particle reactivity and turning off the separation-dependent activity between ZnO and the sulfonated PS. The size of the simulation system is set at roughly 40 times the length of the ZnO nanorod.

exchange between particles. To prove this hypothesis, other ion sources and ion exchangers can be used in place of ZnO nanorod and sulfonated PS microbead. The ion-exchangeable metal-organic framework MIL-101 nanoparticle and $CaCO_3$ microcube were used to replace sulfonated PS and ZnO nanorod, respectively. It is observed that both MIL-101/ZnO and $CaCO_3$/sulfonated PS couples show robust attraction–repulsion interactions via an ion-exchange reaction (Supplementary Fig. 7b,c and Supplementary Video 3).

Swarming behaviour of the active complex

Due to the strong dynamic coupling, the ZnO–sulfonated PS assemblies can further interact with each other and form hierarchical and dynamic swarms. As shown in Supplementary Video 5, on mixing, the sulfonated PS microbeads first accumulate either around or aside the ZnO nanorod by chemotaxis. As more sulfonated PS microbeads accumulate, the diffusion length of Zn^{2+} and OH^- is suppressed, where attractive osmosis drives the sulfonated PS microbead

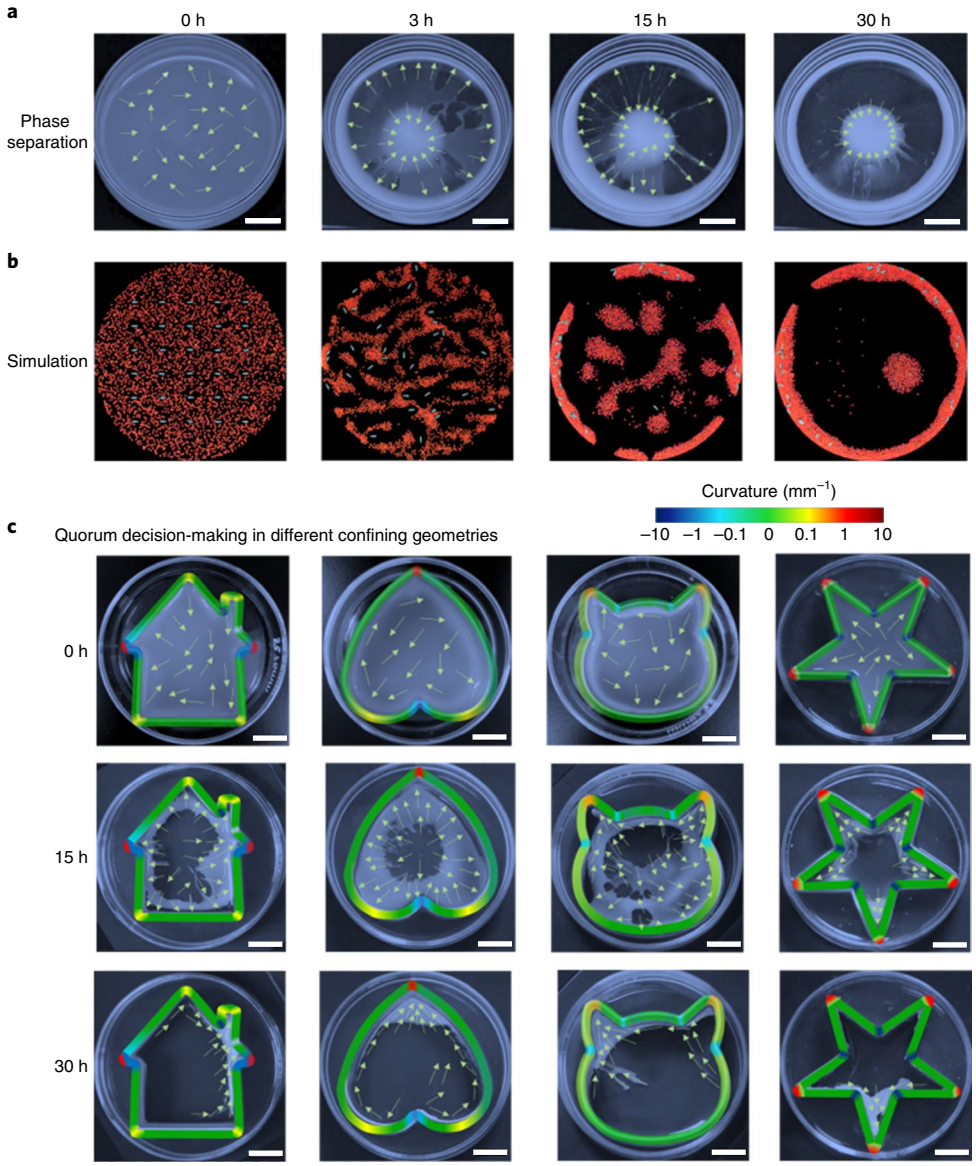

Fig. 5 | Sequential snapshots of macroscopic particle population of ZnO–sulfonated PS mixture in glass petri dishes. a, Phase-segregation behaviour of the ZnO–sulfonated PS active mixture (1 μg ml^{-1} ZnO nanorod and 0.1 mg ml^{-1} sulfonated PS particles) in a round petri dish. **b**, Simulation of a ZnO–sulfonated PS system in circular confinement. **c**, Quorum sensing aggregation with different confined geometries. The house-, heart-, cat- and star-shaped confinements are made from commercial cookie moulds. The yellow arrows represent the migration direction of particles, while the gradient colour outlines indicate the curvature of the confining walls. Scale bars 1 cm (**a**,**c**).

and ZnO nanorod to approach each other (Supplementary Fig. 9), and, consequently, a plethora of tightly bonded ZnO nanorod–sulfonated PS core-shell clusters are formed (Fig. 4a). The pH profile and Zn^{2+} profile of the ZnO–sulfonated PS core-shell cluster clearly show the zonal chemical gradient (Supplementary Fig. 10). Afterwards, attractive osmosis leads to the cohesion of adjacent ZnO–sulfonated PS complexes (Fig. 4b). As multiple complexes group into larger clusters, the attraction is further enhanced due to accumulated H^+, which attracts free sulfonated PS microbeads as well as discrete ZnO–sulfonated PS complexes further away from the large cluster. This long-range attraction, together with the intercluster attraction, aligns the motion of ZnO–sulfonated PS complexes, as evidenced by the long striped marching of the ZnO–sulfonated PS complexes towards the cluster centre (Fig. 4c,d). On an even larger scale, the intergroup attraction leads to further aggregation, as shown in Fig. 4e. With the deformation of the active aggregation, in some local areas, the sulfonated PS cannot completely exchange the Zn^{2+} released from the ZnO core, which results in the repulsion interaction over other clusters as observed in the upper right corner in Fig. 4f. These rich, multiscale dynamics of the ZnO–sulfonated PS system closely mimics the natural swarms,[8,23,24] (Supplementary Video 5). Our system differs from the previously reported collective behaviour of active particles with a single specie[25,26], where active particles form clusters without further merging into large active swarms. We found this multiscale dynamics to be critical for the emergence of macroscopic collective intelligence.

To explain the criteria of the collective behaviour in the ZnO–sulfonated PS system, we adopted a coarse-grained model on the basis of the experimental observation of a two-particle ion-exchange interaction. In this numerical model, three abstractive interactions are considered to represent the complex ion-exchange interaction between ZnO and sulfonated PS microbeads: (1) the excluded

volume interaction between particles, (2) repulsive osmosis due to the ZnO nanorod dissolution and (3) attractive interaction due to the H^+ release from sulfonated PS microbeads by ion exchange, chemotaxis and substrate introduced osmosis. It is important to note that the osmosis interaction does not obey Newton's third law, and the attractive–repulsive osmosis interactions of ZnO and sulfonated PS microbeads is separation-dependent as the local reactant concentration regulates their activity. As discussed previously, the particle activity is regarded as decaying with the square of the separation distance. The detailed definition of the three featured interactions and the establishment of communication-dependent activity coupling is described in the Supplementary Information.

The simulation starts from uniformly distributed particles (Supplementary Video 6 and Fig. 4g) and gradually evolves from small clusters to large swarms, which is consistent with the experimental observation. Notably, the communication-dependent activity, originated from the ion-exchange reaction, shows its importance in continuous evolvement to large active swarms. As the particle activity is fixed by turning off the communication dependence, the particles still cluster into small assemblies; however, the continuous cluster–cluster merging is drastically slowed down and the system 'trapped' in this isolated cluster state (Supplementary Video 6 and Fig. 4h), which is reminiscent of the previously reported collective behaviour without chemical exchange[25–27].

Macroscopic segregation and quorum decision-making

Generally, active particles under confinement can physically interact with the boundary, which results in geometry-dependent phase-separation[28–31]. For the ZnO–sulfonated PS system, the ion-exchange interaction features much stronger coupling and communication-dependent activity, which may lead to the emergence of a more intricate phase separation and collective intelligence. As shown in Fig. 5a and Supplementary Video 7, the ZnO–sulfonated PS mixture demonstrates macroscopic centre-verge phase segregation in a circular glass petri dish (see Supplementary Information for the detailed experimental process). After mixing in the petri dish, the ZnO–sulfonated PS microbead density fluctuates, and voids are formed in the solution. As the aggregation proceeds, the voids expand and colloids are extracted towards the centre and the edge of the petri dish, where streams of colloids are observed resembling the aligned marching behaviour at the microscopic scale shown in Fig. 4d. Finally, the ZnO–sulfonated PS swarm concentrates close to the wall and the centre of the petri dish. In contrast, without ion-exchange interaction, the colloids with only ZnO nanorods, passive PS particles or traditional Janus Pt-based active particles do not show apparent macroscopic phase segregation (Supplementary Fig. 11 and Supplementary Video 7).

The coarse-grained model also reproduces the edge-preferred phase-separation as found in the experiment. In the circular confinement, the wall of the dish (Fig. 5a) suppresses ion diffusion, thus it effectively enhances the ionic concentration near the edges. As shown in Fig. 5b, the particle–edge interaction and the interaction between ZnO and sulfonated PS microbeads promote centre-verge phase segregation, in accordance with our experiment.

Collective intelligence could emerge from the vast networks of components without central control. For instance, microorganisms regulate their behaviour from random to aligned motion by exchanging chemical signals as observed in quorum sensing, where the autoinducer secreted by individual bacteria is sensed by other community members[14,32]. By quorum sensing, bacteria can detect topological defects[33] and can be patterned by confined geometry[34]. Moreover, self-propelled active particles have been investigated to mimic the microbial activities for the study of quorum sensing[35,36]. However, due to weak interparticle communication and lack of particle density regulation, the macroscopic quorum response and consensus decision-making have yet to be observed. In our ZnO–sulfonated PS system, the ion-exchange reaction drives the system far away from thermodynamic equilibrium, while H^+ and Zn^{2+} take the place of the autoinducer in bacteria communication that enables the particle to 'sense' the local population density.

As shown in Fig. 5c and Supplementary Video 8, the circular petri dish is replaced with irregular confining geometries, where the ZnO–sulfonated PS mixture exhibits an intriguing corner-finding ability. The ZnO–sulfonated PS mixture starts from uniform dispersion in four irregular containers (the first row of Fig. 5c), where the curvatures of the edges are highlighted with the colour map. At first, the mixture accumulates towards all edges and corners as expected from geometry-dependent phase segregation. However, as the accumulation continues, the highest curvature corners confine the out-diffusion of ions better, which leads to faster particle accumulation. Once the quorum threshold of colloidal concentration is reached at one particular site due to the swarming fluctuation (the second row of Fig. 5c), the mixture no longer acts autonomously. Instead, the mixture now acts as a united swarm, where almost all colloids start to migrate towards a single accumulated corner, despite some equivalent accumulation sites are also available (such as the other ear vertex of the cat head, and the other four corner vertices of the star). This consensus decision-making behaviour is analogous to the quorum sensing among microorganisms. Eventually, all colloids are confined to a single sharp corner of the container (the bottom row of Fig. 5c), and this pattern can last for several days without diffusion. This quorum sensing-based geometry detection strategy has been proved more efficient compared to other strategies and is adopted by bees and ants during their recolonization[37,38].

To further support the proposed ion-exchange based quorum sensing mechanism, several control experiments were performed by varying the ion-exchange interaction and the local colloidal population (see Supplementary Information for the detailed experiment process and Supplementary Video 7 for experimental results). First, we show the importance of communication-dependent interaction by turning it off with a chelating agent. A low concentration of EDTA solution was added to the ZnO–sulfonated PS mixture, which competed for Zn^{2+} with sulfonated PS microbeads. As the ZnO–sulfonated PS microbead communication was disrupted, the mixture lost the collective decision-making ability where only small scattered clusters were observed (Supplementary Fig. 12a), which was similar to the traditional active particle systems (Supplementary Fig. 11c) and aligned with our simulation results as shown in Fig. 4h. Then, we tried to perturb the macroscopic swarm with preconcentrated particles. As shown in Supplementary Fig. 12b, the preconcentrated sulfonated PS microbeads were placed inside the system, which generated excessive attractive osmosis and promoted particle aggregation to reach the quorum threshold. This preselected high population site outweighed other locations and drove the convergence of the whole colloidal swarm towards it. Finally, a local Zn^{2+} ion source was added to the system, which created repulsive osmosis and jeopardized the colloidal population accumulation (Supplementary Fig. 12c). Eventually, the system reached a consensus to settle away from the local Zn^{2+} source.

Conclusion

In summary, we have shown an ion-exchange interaction between a ZnO nanorod and sulfonated PS microbeads, and the consequent collective behaviour on a hierarchical scale. On mixing the ZnO nanorods and sulfonated PS microbeads, the ZnO–sulfonated PS complex is formed, and intriguing swarming, phase segregation and quorum decision-making behaviours are established from the microscopic to the macroscopic scale. Our numerical model indicates that communication-dependent activity is essential to the emergence of these rich collective behaviours. This result indicates that the ion-exchange reaction could be a versatile tool to construct complex chemical interactions between active particles, which sheds light on understanding and designing new responsive active matters[39].

Online content

Any methods, additional references, Nature Research reporting summaries, source data, extended data, supplementary information, acknowledgements, peer review information; details of author contributions and competing interests; and statements of data and code availability are available at https://doi.org/10.1038/s41565-020-00825-9.

Received: 4 December 2019; Accepted: 25 November 2020;
Published online: 11 January 2021

References

1. West, S. A., Griffin, A. S., Gardner, A. & Diggle, S. P. Social evolution theory for microorganisms. *Nat. Rev. Microbiol.* **4**, 597–607 (2006).
2. Reynolds, C. W. *Flocks, Herds and Schools: A Distributed Behavioral Model* Vol. 21 (ACM, 1987).
3. Bialek, W. et al. Statistical mechanics for natural flocks of birds. *Proc. Natl Acad. Sci. USA* **109**, 4786–4791 (2012).
4. Nelson, B. J., Kaliakatsos, I. K. & Abbott, J. J. Microrobots for minimally invasive medicine. *Annu. Rev. Biomed. Eng.* **12**, 55–85 (2010).
5. Wang, J., Xiong, Z., Zheng, J., Zhan, X. & Tang, J. Light-driven micro/nanomotor for promising biomedical tools: principle, challenge, and prospect. *Acc. Chem. Res.* **51**, 1957–1965 (2018).
6. Wang, J. *Nanomachines: Fundamentals and Applications* (John Wiley & Sons, 2013).
7. Singh, D. P., Choudhury, U., Fischer, P. & Mark, A. G. Non-equilibrium assembly of light-activated colloidal mixtures. *Adv. Mater.* **29**, https://doi.org/10.1002/adma.201701328 (2017).
8. Bechinger, C. et al. Active particles in complex and crowded environments. *Rev. Mod. Phys.* **88**, 045006 (2016).
9. Niu, R. & Palberg, T. Modular approach to microswimming. *Soft. Matter* **14**, 7554–7568 (2018).
10. Miskin, M. Z. et al. Electronically integrated, mass-manufactured, microscopic robots. *Nature* **584**, 557–561 (2020).
11. Handl, J. & Meyer, B. Ant-based and swarm-based clustering. *Swarm. Intell.* **1**, 95–113 (2007).
12. Coyte, K. Z., Schluter, J. & Foster, K. R. The ecology of the microbiome: networks, competition, and stability. *Science* **350**, 663–666 (2015).
13. Faust, K. & Raes, J. Microbial interactions: from networks to models. *Nat. Rev. Microbiol.* **10**, 538–550 (2012).
14. Mukherjee, S. & Bassler, B. L. Bacterial quorum sensing in complex and dynamically changing environments. *Nat. Rev. Microbiol.* **17**, 371–382 (2019).
15. Dag, S., Wang, S. & Wang, L. W. Large surface dipole moments in ZnO nanorods. *Nano Lett.* **11**, 2348–2352 (2011).
16. Zhou, J., Xu, N. S. & Wang, Z. L. Dissolving behavior and stability of ZnO wires in biofluids: a study on biodegradability and biocompatibility of ZnO nanostructures. *Adv. Mater.* **18**, 2432–2435 (2006).
17. Valtiner, M., Borodin, S. & Grundmeier, G. Stabilization and acidic dissolution mechanism of single-crystalline ZnO (0001) surfaces in electrolytes studied by in-situ AFM imaging and ex-situ LEED. *Langmuir* **24**, 5350–5358 (2008).
18. Dey, K. K., Bhandari, S., Bandyopadhyay, D., Basu, S. & Chattopadhyay, A. The pH taxis of an intelligent catalytic microbot. *Small* **9**, 1916–1920 (2013).
19. Tu, Y., Peng, F. & Wilson, D. A. Motion manipulation of micro- and nanomotors. *Adv. Mater.* **29**, https://doi.org/10.1002/adma.201701970 (2017).
20. Niu, R., Palberg, T. & Speck, T. Self-assembly of colloidal molecules due to self-generated flow. *Phys. Rev. Lett.* **119**, 028001 (2017).
21. Niu, R., Fischer, A., Palberg, T. & Speck, T. Dynamics of binary active clusters driven by ion-exchange particles. *ACS Nano.* **12**, 10932–10938 (2018).
22. Soto, R. & Golestanian, R. Self-assembly of catalytically active colloidal molecules: tailoring activity through surface chemistry. *Phys. Rev. Lett.* **112**, 068301 (2014).
23. Bricard, A., Caussin, J. B., Desreumaux, N., Dauchot, O. & Bartolo, D. Emergence of macroscopic directed motion in populations of motile colloids. *Nature* **503**, 95–98 (2013).
24. Vicsek, T., Czirok, A., Ben-Jacob, E., Cohen, I. I. & Shochet, O. Novel type of phase transition in a system of self-driven particles. *Phys. Rev. Lett.* **75**, 1226–1229 (1995).
25. Duan, W., Liu, R. & Sen, A. Transition between collective behaviors of micromotors in response to different stimuli. *J. Am. Chem. Soc.* **135**, 1280–1283 (2013).
26. Altemose, A. et al. Chemically controlled spatiotemporal oscillations of colloidal assemblies. *Angew. Chem. Int. Ed.* **56**, 7817–7821 (2017).
27. Singh, D. P. et al. Interface-mediated spontaneous symmetry breaking and mutual communication between drops containing chemically active particles. *Nat. Commun.* **11**, 2210 (2020).
28. Kudrolli, A., Lumay, G., Volfson, D. & Tsimring, L. S. Swarming and swirling in self-propelled polar granular rods. *Phys. Rev. Lett.* **100**, 058001 (2008).
29. Wensink, H. & Löwen, H. Aggregation of self-propelled colloidal rods near confining walls. *Phys. Rev. E.* **78**, 031409 (2008).
30. Bricard, A. et al. Emergent vortices in populations of colloidal rollers. *Nat. Commun.* **6**, 7470 (2015).
31. Narayan, V., Ramaswamy, S. & Menon, N. Long-lived giant number fluctuations in a swarming granular nematic. *Science* **317**, 105–108 (2007).
32. Whiteley, M., Diggle, S. P. & Greenberg, E. P. Progress in and promise of bacterial quorum sensing research. *Nature* **551**, 313–320 (2017).
33. Peng, C., Turiv, T., Guo, Y., Wei, Q.-H. & Lavrentovich, O. D. Command of active matter by topological defects and patterns. *Science* **354**, 882–885 (2016).
34. Park, S. et al. Motion to form a quorum. *Science* **301**, 188 (2003).
35. Bauerle, T., Fischer, A., Speck, T. & Bechinger, C. Self-organization of active particles by quorum sensing rules. *Nat. Commun.* **9**, 3232 (2018).
36. Solon, A. P. et al. Pressure is not a state function for generic active fluids. *Nat. Phys.* **11**, 673–678 (2015).
37. Pratt, S. C., Mallon, E. B., Sumpter, D. J. & Franks, N. R. Quorum sensing, recruitment, and collective decision-making during colony emigration by the ant *Leptothorax albipennis*. *Behav. Ecol. Sociobiol.* **52**, 117–127 (2002).
38. Visscher, P. K. & Camazine, S. Collective decisions and cognition in bees. *Nature* **397**, 400–400 (1999).
39. Needleman, D. & Dogic, Z. Active matter at the interface between materials science and cell biology. *Nat. Rev. Mater.* **2**, 17048 (2017).

Methods

ZnO nanorod synthesis. The ZnO nanorod array was synthesized following the previous method[40]. A thin layer of ZnO crystal seeds was prepared by depositing 2 nm of Zn on the washed Si wafer (100) through thermal evaporation followed by annealing in air. $Zn(NO_3)_2{\cdot}6H_2O$, methenamine $(CH2)_6N_4$ and polyethyleneimine (branched) were dissolved in deionized water and preheated at 60 °C for 30 min. The preheated solution and the ZnO-seeded Si wafer were sealed and reacted at 95 °C for 5 h. The as-grown nanorods were washed with ethanol and deionized water before measurement. The prepared ZnO nanorod had a diameter of 800 nm and a length of 5–10 μm.

Sulfonated PS microbead synthesis. A two-stage swelling and copolymerization method was used to prepare the crosslinked PS microbeads[41]. Synthesized PS seeds[42] were dispersed in a flask containing SDS solution (0.3% w/w). Then, 200 μl of 1-chlordecone and 8 ml of aqueous SDS were mixed and emulsified by ultrasonication. The emulsion was then added to the particle suspension solution and stirred at 30 °C for 12 h (ref. [43]). Next, 75 mg of azobis (isobutyronitrile) dissolved in 7 ml of styrene and 0.07 ml of divinylbenzene was added. The mixture was purged with nitrogen for 30 min and kept at 78 °C for polymerization for 12 h. The obtained particles were washed with deionized water and freeze dried. Crosslinked PS particle powder (1 g) was sulfonated with concentrated sulfuric acid (98%, 50 ml) at 50 °C for 12 h. After being cooled down to room temperature, the obtained sulfonated PS particles were collected by centrifugation and repeatedly washed with a large excess of ethanol.

3D velocity field measurement. The ZnO nanorod was fixed at the glass substrate by fast drying the ZnO colloid on the glass substrate. The glass substrate was covered with a polydimethylsiloxane chamber filled with sulfonated PS colloid. The microscope was focused at different depths ($Z = 0$, 6, 10, 14 μm) and trajectories of sulfonated PS particles at each depth layer were tracked. Here, 400 trajectories and 5,500 data points of sulfonated PS were tracked at four depth layers. The 3D coordinates and velocity data were then processed using MATLAB to get the 3D velocity field.

In situ pH profile mapping. Here, 2 mM 5(6)-carboxyfluorescein (5(6)-CF) stock solution in deionized water was prepared and kept at 4 °C in the dark and used for several weeks. Series of pH solutions without zinc ions added (range from 3 to 10) were prepared. Then, 0.5 μM 5(6)-CF was applied to calibrate the relationship between fluorescent intensity and pH[44]. For 0.5 μM 5(6)-CF in deionized water, the excitation wavelength was set at 488 nm, and the fluorescence emission spectrum was recorded between 500 and 600 nm ($\lambda_{max} = 518$ nm). Fluorescence of 5(6)-CF solution at each pH value was collected by using a confocal laser scanning microscope (LEICA TCS SP8) with an excitation wavelength $\lambda_{ex} = 488$ nm and acquisition wavelength between 500 and 600 nm. The calibration curve was obtained by scanning the standard pH solution. The calibration experiment and pH mapping were conducted at the same setting parameters.

Macroscopic phase separation and quorum decision-making. The as-grown sulfonated PS particles were thoroughly washed with deionized water until pH 7.0 and the ZnO nanorods were cleaned in oxygen plasma for 3 min to remove any attached organic residuals. The sulfonated PS colloid (0.1 mg ml^{-1}) and ZnO nanorod (1 μg ml^{-1}) were mixed in deionized water and sonicated at 25 °C for 15 min. The well-mixed suspension was then poured into 6-cm diameter glass petri dishes. The phase-separation processes were captured by a digital camera at 5 s per frame. To verify the necessity of ion-exchange reaction for the emergence of the collective motion and macroscopic phase-separation, three control experiments were conducted in the same experimental procedure by using the ZnO nanorods, passive PS microbeads and Janus Pt-TPM Janus microspheres to replace the ZnO–sulfonated PS mixture. All systems were monitored for 30 h.

For the quorum decision-making experiment, the cookie moulds were placed in the middle of glass petri dish, while the region outside the moulds was sealed by pouring polydimethylsiloxane and then allowed to cure at 75 °C. The ZnO–sulfonated PS mixture was then poured in the cookie mould patterns. The quorum decision-making process was monitored by a digital camera at 5 s per frame for 30 h.

Janus active particle synthesis. The 1.8-μm diameter TPM particles were prepared following a previous report[45]. After repeated washing and centrifugation, 90 μl of ethanol solution containing TPM particles (10 mg ml^{-1}) was dropped onto a glass slide to form a particle monolayer after ethanol evaporation at 95 °C. Then 10 nm of Pt was deposited onto the TPM particles by magnetron sputtering to produce a Janus structure. The as-prepared Pt/TPM Janus microspheres were scraped off from the substrate with a razor blade and transferred into 2.5 wt% H_2O_2 solution containing 0.3 μg ml^{-1} of PS microbeads as passive particles, which served as the model system for the active–passive particle system.

MIL-101 (Fe) and $CaCO_3$ particle synthesis. The synthesis of MIL-101 (Fe) is based on a reported method[46]. A mixture of terephthalic acid (0.166 g) and $FeCl_3{\cdot}6H_2O$ (0.540 g) in dimethylformamide (40 ml) with 5 M hydrofluoric acid aq. (50 μl) was put in a Teflon-lined stainless-steel autoclave at 383 K for 24 h. The product was collected by repeatedly washing with methanol.

The $CaCO_3$ microcube is synthesized following a previously reported method[47] with slight modifications. In a typical synthesis, Na_2CO_3 (0.5 M) solution was injected quickly into the well-mixed solution of $CaCl_2$ (0.5 M) and starch (0.25 wt%) under vigorous stirring. The product was collected by washing with deionized water and centrifugation.

Data availability

The data that support the plots within this paper and other findings of this study are available from the corresponding author upon reasonable request. Source data are provided with this paper.

References

40. Greene, L. E. et al. Low-temperature wafer-scale production of ZnO nanowire arrays. *Angew. Chem. Int. Ed.* **42**, 3031–3034 (2003).
41. Wang, Y. et al. Synthetic strategies toward DNA-coated colloids that crystallize. *J. Am. Chem. Soc.* **137**, 10760–10766 (2015).
42. Qi, G. et al. Facile and scalable synthesis of monodispersed spherical capsules with a mesoporous shell. *Chem. Mater.* **22**, 2693–2695 (2010).
43. Gibson, H. W. & Bailey, F. C. Chemical modification of polymers. 13. Sulfonation of polystyrene surfaces. *Macromolecules* **13**, 34–41 (1980).
44. Massou, S., Albigot, R. & Prats, M. Carboxyfluorescein fluorescence experiments. *Biochem. Educ.* **28**, 171–173 (2000).
45. Van der Wel, C. et al. Preparation of colloidal organosilica spheres through spontaneous emulsification. *Langmuir* **33**, 8174–8180 (2017).
46. Li, B. et al. Metal-organic framework based upon the synergy of a Bronsted acid framework and Lewis acid centers as a highly efficient heterogeneous catalyst for fixed-bed reactions. *J. Am. Chem. Soc.* **137**, 4243–4248 (2015).
47. Wei, W. et al. Preparation of hierarchical hollow $CaCO_3$ particles and the application as anticancer drug carrier. *J. Am. Chem. Soc.* **130**, 15808–15810 (2008).

Acknowledgements

This work was supported in part by the Innovation and Technology Commission (HKSAR, China) to the State Key Laboratory of Synthetic Chemistry, and the Hong Kong Research Grants Council General Research Fund (grant nos. GRF17305917, GRF17303015 and GRF17304618), the Seed Funding for Interdisciplinary Research (University of Hong Kong), the URC Strategic Research Theme on New Materials (University of Hong Kong), the Science Technology and Innovation Programme of Shenzhen (JCYJ20170818141618963), the Shenzhen-Hong Kong Innovation Circle Programme (SGDX2019081623341332) and the National Natural Science Foundation of China (no. 11874397).

Author contributions

C.W. and J.T. conceived and designed the project. C.W., J.D., L.G. and J.L. prepared the samples. C.W., J.D. and J.T. conducted most of the measurements and analysis. X.L. helped with COMSOL simulation. M.Y. performed the coarse-grained simulation and analysis. C.W. and J.T. wrote most of the manuscript. J.D. and M.Y. participated in the manuscript revision. All authors discussed the results and commented on the manuscript.

Competing interests

The authors declare no competing interests.

Additional information

Supplementary information is available for this paper at https://doi.org/10.1038/s41565-020-00825-9.

Correspondence and requests for materials should be addressed to M.Y. or J.T.

Peer review information *Nature Nanotechnology* thanks the anonymous reviewers for their contribution to the peer review of this work.

Reprints and permissions information is available at www.nature.com/reprints.